Intensifying tropical cyclones associated with more frequent hazardous material pipeline failures

M. Smith[1] and E. Carter[2,*]

[1] *Civil and Environmental Engineering, Cornell University, Ithaca, NY 14850, USA*
[2] *Civil and Environmental Engineering, Syracuse University, Syracuse, NY 13244, USA*
[*] *corresponding author, ekcarter@syr.edu*

December 3, 2024

Abstract

Over 30,000 hazardous material pipeline (HMP) failures have been reported in the US since 1970, associated with 274 fatalities, 1,120 injuries, and nearly $11 billion in damages. Tropical cyclones are under-recognized as drivers of pipeline failures, mainly because failures aren't associated with tropical cyclones on operator-generated incidence reports, limiting analysis. This study defines tropical cyclone-associated pipeline failure frequency using a conservative framework based on spatiotemporal concomitance with the tropical cyclone storm tracks. A modeling framework that accounts for unparameterized spatial and temporal non-independence in HMP failure frequency, as well as collinearity in meteorological metrics of tropical cyclone intensity, is used to evaluate spatiotemporal variability in local HMP failure frequency associated with variable tropical cyclone intensity. Over 70% of reported pipeline failures in tropical cyclone-active regions occur within the first year of a tropical cyclone exposure. Since 1975, the annual frequency of tropical cyclone-associated pipeline failures has increased by an order of magnitude. Storm intensity (minimum pressure and maximum wind speed) is significantly related to the number of pipeline failures associated with a storm, explaining 24% of spatial variability and 34% of inter-annual variability in local storm-level pipeline failure frequency. Pipeline systems in the Texas Gulf Coast, Mississippi Delta Region, Northeast, and High Plains regions are most susceptible to tropical cyclone-associated failures. Assuming linear continuations of meteorological trends observed in 1970-2020, our results suggest that we may see a 50-600% increase in the number of pipeline failures occurring during the local annual average maximum tropical cyclone by 2050. Implications of accurate natural hazards-related cause attribution on HMP failure incident reports are discussed.

1 Introduction

The United States' onshore hazardous material pipeline (HMP) network, spanning over 3.3 million miles, is a critical component of the nation's transportation infrastructure. The majority of petroleum products used for energy production in the United States are transported through this HMP network, and national dependence on HMPs has driven a nearly 14% expansion of the network in the past eight years (Parfomak 2023) with an almost 30 million barrels per day increase in usage projected by 2040 (International Energy Agency 2016). Despite the benefits of HMP infrastructure, failures in this network are associated with devastating economic, environmental, and social costs (Li *et al* 2022). HMP failures cause large volumes of petroleum products to be released into the environment, leading to persistent contamination of surface water, soil, and groundwater (PHMSA 2023). Over 30,000 HMP failures have been reported in the United States since 1970. Between 2005-2023, reported HMP failures were associated with 274 fatalities, 1,120 injuries, and nearly $11 billion in damages (PHMSA 2023). Between 28-95% of the total costs of pipeline failures are associated with environmental damage and remediation (Restrepo *et al* 2009, Belvederesi *et al* 2018), yet even with the large price tag associated with remediation, about 85% of products released remain unrecovered after the accident (Belvederesi *et al* 2018, Maxwell *et al* 2018), leading to long-lasting ecological and public health impacts.

In 1968, the Pipeline Safety Act mandated and outlined the requirements for reporting hazardous material pipeline (HMP) failures (U.S. Department of Transportation 2021, Armstrong 1969). This regulation requires pipeline operators to report incidents within 30 days of occurrence, providing accident-specific details such as location, facilities involved, operations, personnel conduct, and the cause of the incident. When reporting pipeline failures, pipeline operators attribute failures to a single cause from pre-defined categories such as corrosion, excavation damage, external forces, material or weld failures, equipment malfunctions, incorrect operation, or natural forces (added in 2002) (Text S1). Yet, in reality, HMP failures frequently result from the interaction of multiple contributing factors. This narrow attribution approach weakens the effectiveness of risk assessments, which rely on public datasets like PHMSA's to model failure frequency and causes (Zakikhani *et al* 2019, Ricci *et al* 2021). The inability to account for multifaceted drivers in a single-cause framework limits the precision of risk models in accurately quantifying the probability and impact of failures (Lam and Zhou 2016).

Though estimates vary widely, meteorological events, specifically tropical storms and hurricanes (tropical cyclones, TCs), are reported to contribute significantly to total damages associated with natural-hazard triggered pipeline accidents in the United States (Girgin and Krausmann 2014), and have been estimated to be the cause of up to 86% of all natural-hazard mediated pipeline failures worldwide (Ricci *et al* 2021). While the true magnitude of natural-hazard-associated pipeline failures is likely underestimated due to reporting bias (Girgin and Krausmann 2015), TCs are broadly understood to be an important,

and under-characterized, driver of HMP failures (Ricci *et al* 2021, Girgin and Krausmann 2015).

As average ocean temperatures across the Atlantic Basin continue to increase due to climate change (Abraham *et al* 2013), TCs, which are fueled by warm ocean temperatures, have shown a commensurate increase in intensity and frequency (Vecchi *et al* 2021). Guzman et al. (2021) documented a 1.3% increase in TC precipitation intensity per year from 1998-2016. During the historic 2020 hurricane season, a 0.4-0.9°C sea surface anthropogenic sea surface temperature anomaly in the Atlantic Basin was directly associated with a 10% increase in 3-hourly rainfall intensity during TCs (Reed *et al* 2022). Studies show that the most damaging tropical cyclones—those categorized as three or higher—are responsible for approximately 85% of the total TC damages, even though they constitute 24% of landfalling storms (Jr *et al* 2005). These extreme events are particularly challenging to simulate accurately in gridded climate models (Mallard *et al* 2013), leading to inconclusive findings in numerical studies regarding the effects of anthropogenic climate change on the frequency and intensity of the most powerful TCs. However, historical data analysis indicates a significant rise in the occurrence of these high-intensity storms in particular (Vecchi *et al* 2021, Ricci *et al* 2021).

Regulatory bodies across the world target HMP design standards on building network resilience to natural disasters, such as earthquakes in California (Nair *et al* 2018) and tsunamis in Japan (Murphy and Conner 2012). TC storm tracks impact 19 US states, overlapping with some of the densest HMP infrastructure in North America (Safety and Certainty 2023).TCs can stress pipeline systems through a variety of mechanisms, including but not limited to mechanical stress from high wind speeds; intense precipitation and related impacts including compound flooding; soil shifting and settling; erosion, accretion, and landslides; storm surges and related coastal impacts; and intensified tornado activity inland (Czajkowski *et al* 2011, 2017, Qin *et al* 2020a, Burow *et al* 2021). Some of these stresses are acute, and can logically be associated with pipeline failure at low latency to the forcing. For example, TC-associated tornado damage to an above-ground transmission pipeline is easily attributable to an individual storm event. Many of these stresses are cumulative and can result in a decreased overall lifetime of the pipe system. For instance, a pipeline network subject to frequent bouts of wetting and drying due to TC-related precipitation in regions with high shrink-swell potential could undergo significant mechanical stress; and pipelines impacted by saline storm surges coastally could experience more rapid rates of corrosion over time.

To inform dialogue on engineering standards for HMP failure reporting, design, and maintenance in hurricane-prone regions in the 21st century, the objective of this study is to quantify trends in HMP failure associated with observed increases in TC intensity (TCI) associated with climate change. As there are no historical records of TC associated storm failures available through the PHMSA, a conservative framework to relate HMP failures to specific TCs is proposed. Utilizing a simple modeling framework that can control for, and quantify the relative importance of, unparameterized non-meteorological spatiotemporal drivers

of HMP failure **carter2023grrien**, we estimate the extent to which increases in TCI observed in the last 50 years are associated with increased TC failure frequencies during the same time period. We confirm conclusions from other analysis suggesting that the average annual maximum storm intersecting with HMP infrastructure has increased from a Cagtegory 3 in 1970 to a Category 4 in 2010. In the absence of robust numerical models, we must extrapolate from this trend to assume a linear increase in TCI in the 21st century, implying that the average annual maximum storm intersecting with HMP infrastructure will be a Category 5 by 2050. These results underscore the significance of meaningful design interventions to stabilize HMPs in TC regions, and confirm conclusions from previous studies suggesting that HMP failures associated with TCs are likely under-reported.

2 Methods

2.1 Data Preparation

This analysis aims to identify TC-associated pipeline failures in the PHMSA database (PHMSA 2013). Prior to 2002, "natural force damages" was not a causal category on incident forms, and post-2002, there is suggested negative reporting bias to this causal category (Text S1, Figure S1). In line with standards established in **carter2023grrien**, all data and code comprising this analysis are available online (see SI). We examine intersections between PHMSA Failure Data (HMP failures) and 6-hourly points in the NOAA HURDAT2 Dataset (TC points), (National Hurricane Center 2023, PHMSA 2023). We merge the datasets by identifying records where HMP failure coordinates fall within the TC point force diameter or, when the force diameter is unavailable, within 300 miles (the average TC for of the TC point. Additionally, the failures must occur within 60 days of the TC point intersection. Before merging, all HMP failures and TC points that fall outside the North American TC storm track region are discarded. Each hurricane is assigned a unique identifier combining the storm name and year (e.g., 'StormNameYYYY') to account for repeated names across different years. If HMP failures do not intersect with any TC points, they are associated with a 'NoStormYYYY' identifier, where 'NoStorm' signifies HMP failure in the absence of a corresponding TC. Likewise, TC points that do not intersect with HMP failure points are retained with no affiliated failure points. The merged TC x HMP dataset therefore includes three types of records (Text S1, Figure S2):

1. HMP failure associated with a TC: a value of 1 is assigned to associated storm ID Note: storm ID records are repeated for each unique TC point intersection, ensuring that multiple intersections with the same storm are fully captured.

2. HMP failure unassociated with a TC: a value of 1 is assigned with annual 'NoStorm ID. Note: NoStorm ID records are replicated for each unique

HMP point intersection.

3. TC associated with no HMP failures (a value of 0 is assigned with a storm ID).

To account for regional variations in hazardous material pipeline (HMP) failure rates due to factors unrelated to tropical cyclones (e.g., local pipeline construction practices, network length and density, network age, ambient geophysical conditions, and use characteristics), we applied k-means clustering to define six spatial sub-regions based on the most precise latitude and longitude available for each record in the tropical cyclone TC x HMP dataset (Text S1, Figure 1, Pedregosa *et al* 2011). The merged TC x HMP dataset is then aggregated by summing on storm name and region, providing the frequency of pipeline failures per storm, per location, and per year (f_s). Included in f_s is the annual total number of failures unassociated with a TC (the sum of the "NoStormYYYY" variable). To control for trends in pipeline failures not associated with TCs (e.g., increasing pipe age, increasing pipe length), the 5-year 60-day average "NoStorm" failure frequency (f_o) for each sub-region ($j = 1, \ldots, 6$) for each five-year period ($y = 1, \ldots, 10$) between 1972 and 2022 is then calculated and subtracted from each storm-associated frequency ($f_s^{(i,j,y)}$), resulting in the storm-related failure frequency ($f_s'^{(i,j,y)}$, Eq 1):

$$f_s'^{(i,j,y)} = \max\left(f_s^{(i,j,y)} - f_o^{(j,y)}, 0\right) \tag{1}$$

2.2 Model Fitting

Due to the multilevel nature of the data and the presence of zero values in f_s', we employed strategically nested binomial (Text S2) and Poisson mixed-effects models (Text S3, Eq. 2 and 3). These models used TC intensity (TCI, derived as the first principal component of regional maximum TC wind speed and regional minimum TC pressure) as the main predictor variable (Eq 2, Text S4, Figures S3, S4).

$$\log(\lambda_{ijk}) = \beta_0 + \beta_1 TCI_{ijk} + u_j + v_k + \gamma_j TCI_{ijk} + \epsilon_{ijk} \tag{2}$$

Where λ_{ijk} is the expected storm HMP failure frequency for the i-th storm in the j-th region and k-th year, TCI_{ijk} is TC intensity for the i-th storm in the j-th region and k-th year, β_0 is the overall log-rate intercept. β_1 is the fixed log-rate coefficient for the predictor TCI_{ijk}, u_j is the random intercept for region j, capturing the residual deviation of the j-th region from the overall intercept, v_k is the random intercept for year k, capturing the residual deviation of the k-th year from the overall intercept, γ_j represents the random log-rate coefficient local to each region j, and ϵ_{ijk} is the residual error term. The "full" model (Eq 2) is compared to a null model with no fixed effects (Eq 3):

$$\log(\lambda_{ijk}) = \beta_0 + u_j + v_k + \epsilon_{ijk} \tag{3}$$

4

The panel model structure mitigates variance bias associated with omitted variables and non-independence of observations (**carter2023grrien**; **f2007methods**), and the nested panel model structure (comparing Eq 1 to Eq 2) enables a more detailed examination of how temporal (year) and spatial (region) variability in f'_s is influenced by TCI, The model assumes variance component partitioning between random effects, where $u_j(i) \sim \mathcal{N}(0, \sigma_j^2)$, $v_k(i) \sim \mathcal{N}(0, \sigma_k^2)$, and $\epsilon_{ijk} \sim \mathcal{N}(0, \sigma_\epsilon^2)$ (Text S5, S6).

2.3   Estimating Trends and Future Predictions

Historical trends in annual TC minimum pressure and maximum wind speed (1970–2022) were analyzed using OLS regression. We make a simplified, but necessary, assumption that the linear trends will remain constant until 2050 (Text S7), and use these models to estimate the 1970, 2010, and 2050 annual maximum TC wind speed and minimum pressure, both globally and for each region (Figure S5). These values are converted to the 1970, 2010, and 2050 TCI using the principal components model trained on historical TC data. TCI values input into the trained Poisson mixed-effects model (Eq 2) to predict storm-associated failure frequency (f'_s) associated with the regional annual maximum TCI for 1970, 2010, and 2020.

3   Results

3.1   Pipeline Failure Attribution Analysis

Between 1986 and 2022, pipeline failures in the PHMSA dataset were categorized as resulting from natural forces (4.3%, or 275 failures), human error (14.9%, or 943 failures), and external forces (80.8%, or 5,124 failures). The first recorded pipeline failure attributed to "natural forces" appeared in 2002, with no significant positive or negative trends in the frequency of this attribution observed since then (Figure S1). In contrast, significant ($p < 0.01$) positive trends were noted in the annual frequency of failures attributed to human error (an increase of 1.33 failures per year) and external forces (an increase of 1.45 failures per year) over the same period (Figure S1). Most "natural forces" failure attributions occurred in Texas, Oklahoma, Louisiana, Illinois, Pennsylvania, and New York (Figure S1).

Since 1970, 870 tropical cyclones (TCs) in the NOAA HURDAT2 database have intersected with HMP infrastructure. Although PHMSA reports attribute a relatively low percentage of pipeline failures to "natural forces," our analysis found that 70% of all PHMSA-reported pipeline failures within the reach of tropical cyclones occurred within one year of overlapping with a HURDAT2 data point. Over the study period, we observed a significant positive linear trend in the annual frequency of failures occurring within 60 days of TC exposure (f_s). Drawing from this trend, in 1975, the annual mean was 4 TC associated failures; by 2020, this number had risen to 50 failures per year (Figure S6). Anomalies
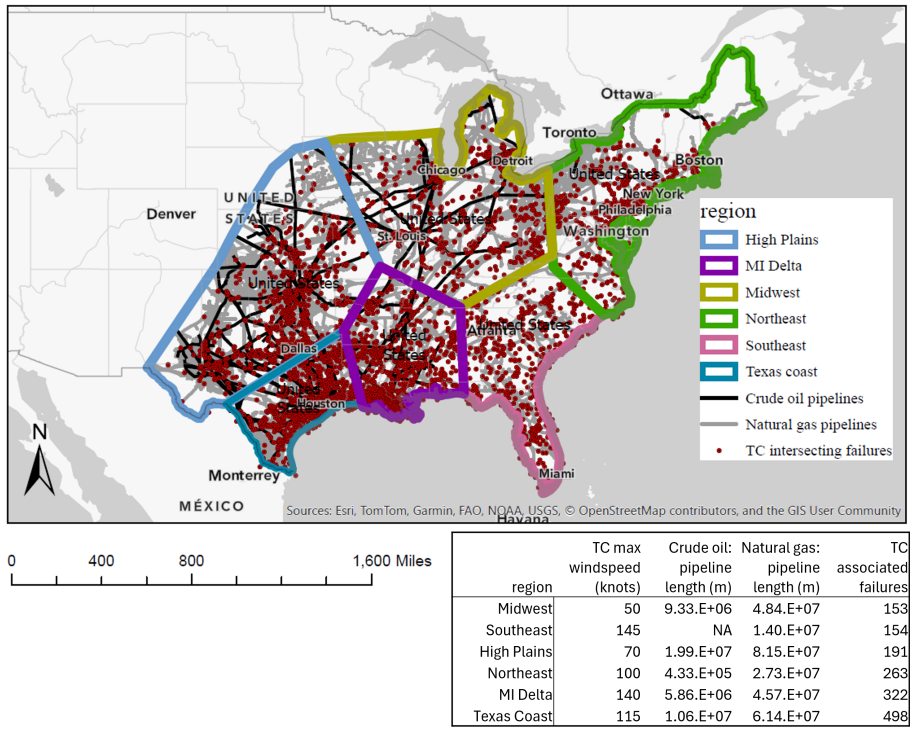
Figure 1: Six regions where HMP infrastructure (major crude oil and natural gas transmission pipelines, EIA 2020) intersect with tropical cyclone storm tracks in the continental United States.For each region, table indicates total 1970-2022 f'_s, maximum TC windspeed, length of crude oil pipeline, and length of natural gas pipeline.

in v_k can be clearly traced to specific storm events (Text S9).

Most of f'_s occurred along the Texas coast, followed by the Mississippi Delta and Northeast regions (Figure 1), where high-magnitude TCs (indicated by wind speed) intersect with dense crude and natural gas pipelines. More frequent f'_s are observed in the second half of the study period relative to the first in the MI Delta and Texas coast, indicative of a stronger trend in these regions (Figure 1). Higher pipeline failure per unit length of crude oil pipeline is observed in the Northeast than other regions (Figure 1). High magnitude f'_s is observed in High Plains, despite lower maximum TC wind speed (Figure 1). The Southeast returns few f'_s relative to high TC wind speeds, likely associated with a lack of crude oil pipeline infrastructure in the region (Figure 1). In the Midwest, where lowest TC wind speeds are observed, as well as in Northeast, the majority of f'_s occurred in 1979 (Figure 2, Figure S7).

TCI is a statistically significant predictor of one or more HMP failures for a given region (α=0.05), with the likelihood of one or more failure increasing

Figure 2: Time series of f'_s by region

by 59% for a standard deviation increase in TCI (Text S7, Figure S8a). TCI explains minimal inter-annual variance (v) in the likelihood of one or more HMP failure (0.2%), but explains 21.8% of the variance in region (u) (Figure S8b,c).

Nested mixed-effects Poisson regression models were fit to capture the frequency of HMP failures associated with a TCI in a given region. In the null model, inter-annual variance in f'_s (v) was 141% greater than regional variance (u) reinforcing that inter-annual variability in f'_s for a given location is greater than regional variability in f'_s within a given year. TCI is a statistically significant (alpha ¡ 0.001) predictor increased frequency of pipeline failures f'_s, explaining 24% of residual variance in u and 34% of residual variance in v (Figure 3a, Text S8).

Shifts in random intercept values for each year and location between a null model (no fixed effects) and the full model (containing TCI as a fixed effect) elucidate the local (to space and time) nuances of how f'_s responds to TCI (Figure 3). In the null model, the highest u_j is observed along the Texas Coast, followed by the Mississippi Delta and the High Plains. The lowest u_j, corresponding the lowest f'_s for a given TC, are observed in the Southeast and in the Midwest. Negative shifts in u_j in the Texas Coast and MI Delta with TCI parameterized suggests that a substantial portion of increased f'_s in this region is explained by increased TCI in the region. A negative shift in u_j in the High Plains suggests that the global coefficient on TCI may lead to an underestimation of TC-associated pipeline failures (f'_s) for increasingly intense TC (Fig 3b). A positive shift in the negative u_j in the Midwest suggests that lower (f'_s) in the region is partially explained explained by lower TCI in the Midwest, relative to other regions (Figure 3b).

The random intercept on year (v_k) in the null model likewise indicates the relative anomaly in (f'_s) for a given year. Evaluating the color scale, we observe 14 out of 20 of the latest years (2002-2022) with a positive v_k, and only 6 out of the 20 latest years with a negative v_k, indicating a trend towards increasing (f'_s) over time. Reduction in the absolute value of v_k between null and full models indicate years when TCI explains anomalies in (f'_s). Strong negative shifts are observed in positive intercepts in 2014, 2005, 2017, 1992, and 2012, suggesting that TCI explained more of the anomalously high (f'_s) in these years (Figure 3c,Text S9).

3.2 Trends in Tropical Cyclone Dynamics

Since 1975, there has been a significant increase in annual maximum TC wind speed of approximately 0.6 knots per year, and a decrease annual minimum TC pressure (indicating increased storm intensity) by -0.7 mBar per year (Fig 4a-b). Drawing from these trends, the annual maximum wind speed and pressure of an Atlantic TC in 1970 was approximately 107 knots and 954 mBar, respectively; corresponding to a Category 3 hurricane on the Saffir-Simpson Hurricane Scale. In 2010, the annual maximum wind speed and minimum pressure of a TC intersecting with HMP infrastructure were 130 knots and 928 mBar, respectively; corresponding to a Category 4 hurricane. Projecting this trend to
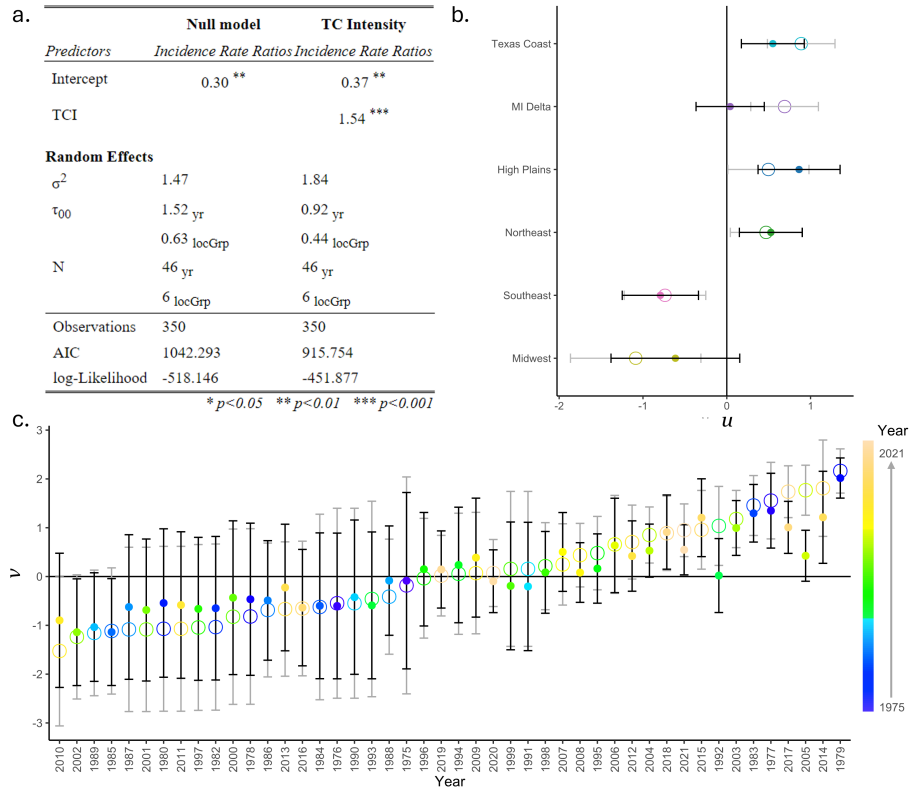
Figure 3: a) Mixed-effects Poisson model parameters and statistics for null (no fixed effects) and full (TCI as a fixed effect) models, b) caterpillar plot of random intercept (points) on location for null (open circles) and full (closed circles) models, with error bar representing 95% confidence interval; color scale indicating location group c) as in b but for random intercept on year, with color scale indicating advancing year.
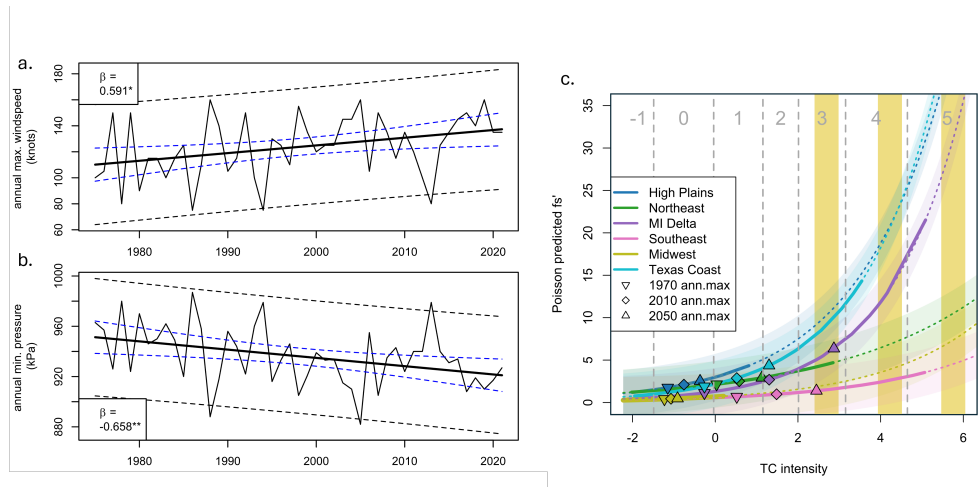
9

Figure 4: Linear trends in 1975-2022 annual maximum HMP intersecting TC windspeed (a) and minimum pressure (b). c) Poisson projected (Eq 2) per-storm pipeline failures for each region (color) with historical range of TCI indicated by solid lines and out-of-sample projections indicated with dashed lines. Inverted triangle, diamond, and triangle symbols correspond to the annual maximum regional TCI projected from linear trends (Fig S5). Yellow bars represented maximum projected HMP intersecting TCI for 1970 (left), 2010 (center), and 2050 (right); extrapolated from linear trends observed 1975-2022 (Figure 4a, b). Dashed vertical lines represent storm classification thresholds on the Saffir-Simpson Hurricane Scale, with corresponding storm classification indicated as text along top of figure.

2050 produces an estimated annual maximum wind speed and minimum pressure of 154 knots and 902 mBar, respectively; corresponding to a Category 5 storm (Figure 4c, yellow bars). Incidentally, significant southeastern shifts in annual maximum TC origin (corresponding to a 0.15 degrees/year southerly and 0.41 degree/year easterly shift) were also observed, consistent with the literature (e.g **knutson˙tropical˙2019**, Figure S10).Projected maximum annual TCs represent the highest-magnitude storm that could be expected to impact the Gulf Coast regions (Texas coast, MI Delta, and Southeast) on an annual basis, and corresponding f'_s are indicated on Figure 4c.

Greatest trends in annual maximum TCI are observed in the MI Delta, with the projected annual maximum intersecting TCI increasing from a category 0 in 1970 to a category 3 in 2050. This is followed by the MI Delta region (with a projected shift from a category 0 to category 3 annual maximum TC between 1970 and 2050), Southeast coast (category 1 to category 3), and Texas coast (category 0 to category 2) (Figure 4c). Projecting from local trends in TCI, the MI Delta and Texas Gulf Coast regions are projected to see an over 5-fold increase in the frequency HMP failure associated with the local annual

maximum TC (f'_s); the High Plains is projected to see a four-fold increase in f'_s by 2050, the Northeast a nearly 3 fold increase in f'_s, and the Southeast and Northeast are expected to see a doubling f'_s per local annual maximum TC by 2050 (Table 1). Drawing from the upper and lower confidence intervals of projections suggests an approximate range of 50-600% increase in HMP failure frequency associated with the local annual maximum TC in 2050.

Region	1970	2010	2050
Midwest	2	4	7
Southeast	2	3	5
High Plains	10	21	42
Northeast	4	7	11
MI Delta	6	13	31
Texas Coast	9	21	46

Table 1: Projected annual maximum f'_s by region and year

4 Discussion

While impacts of damaging wind speeds and intense rainfall are universal, TCs have different impacts on different regions of the United States. Coastal regions (Texas Coast, MI Delta, Southeast Coast) will experience effects of storm surges (Girgin and Krausmann 2015, Sengul *et al* 2012); flat regions (High Plains, Southeast Coast, Midwest) may see tornado activity (Girgin and Krausmann 2016; Edwards 2012) and riverine flooding (Luca *et al* 2017); hilly regions (Northeast) may see compounding flooding, including coastal, riverine, and flash flooding and landslides (Booth *et al* 2021, Lai *et al* 2021); and the High Plains, Texas, and Mississippi Delta region will likely be impacted by high shrink-swell potential of local soils saturated with intense rain (Olive *et al* 1989). As such, it is unlikely that the impacts of TCs on HMP infrastructure will be consistent from place to place. Likewise, there are multiple potential pipeline-side drivers of increase in f'_s over time that are independent of increasing TC intensity, most notably increasing age of pipeline infrastructure and expanding networks (meaning that TC associated pipeline failures are more likely simply because there is more pipeline to fail). Reports of HMP failures due to all causes have increased markedly in the last fifty years (Figure S1), indicating the growing scope and vulnerability of this essential infrastructure system. Most pipelines in operation today have surpassed 45 years of service, a threshold associated with greater risk of failure (Awuku *et al* 2023).

HMP failures associated with TCs (f'_s) are most likely in the MI Delta, followed by the Texas Coast and Northeast (Figure S5); and most frequent on the Texas Coast, followed by the MI Delta, These areas exhibit heightened vulnerability due to dense pipeline networks, high shrink-swell potential of local soils, and exposure to coastal storm surges and high-intensity TCs (Restrepo *et*

al 2009, Girgin and Krausmann 2015). Similar frequencies of f'_s are observed in the High Plains and Northeast (Figure 3b). Increased frequency of f'_s associated with even small shifts in TCI in the High Plains may indicate sensitivity of HMP infrastructure to the impacts of TC-associated tornado activity and high shrink-swell potential of local soils, which can put significant mechanical stress on underground pipeline networks (Clayton *et al* 2010). The lowest number of pipeline failures per TC (f'_s) are observed in the Midwest, followed by the Southeast, likely because of low TC exposure (Midwest) and a lack of crude oil infrastructure in the area (Southeast) (Figure 1, 3b).

Ultimately, our results indicate significant increasing trends in TC associated HMP failure across the United States, and suggests that these increases are associated with both increased vulnerability of HMP infrastructure to TC impacts (indicated by linear trends in v_k), and increasing intensity of TCs intersecting with HMP infrastructure (indicated by linear trends in TCI). Frequency of HMP failure associated increases rapidly for storms greater than Category 3 across all regions (Figure 4c, Figure S7), underscoring the significance of increased risk of major hurricanes in particular, as opposed to risk from increased TC frequency in general, in terms of implications for the resilience of HMP infrastructure in the eastern United States under climate change. Linear trends in TCI noted here are both notable in terms of their magnitude and in terms of their consistency with previous research (Holland and Bruyère 2014, Kossin *et al* 2020, Elsner 2006, Gilford *et al* 2024). Still, physical evidence supporting linear increases in TCI due to global warming is inconclusive; as such, statistical projections of increasing TCI represent a fundamental limitation of this work (Knutson *et al* 2019, Kossin *et al* 2020).It is likewise important to note that caution should be exercised in projecting f'_s beyond the range of TCI observed in each region, as such we do not report projections for f'_s for any region under the projected 2050 global annual maximum storm (yellow bars, Figure 4c).

Although natural force damage accounts for only 4.3% of total failures in the PHMSA dataset, we identified that 32.47% of failures in US regions impacted by TC storm tracks occur within 60 days of a TC intersection, after detrending for non-storm associated failure rates, providing new data to back previous claims in the literature of under-reporting of TC-related HMP failures (Girgin and Krausmann 2015). Given that pipelines often fail due to multiple contributing factors, the current reporting framework that allows for only one primary cause may underestimate the true impact of TCs on pipeline integrity. Given the costs of HMP failures in terms of health, environment, and economic damages, identifying HMP failures associated with TCs are critical to administration of appropriate relief during national emergencies, as well as to improving the accuracy of our accounting of financial damages associated with TC events. Addressing limitations in natural disaster attribution in HMP failure reporting could therefore improve the accuracy of risk assessments and inform better mitigation strategies.

5   Conclusions

Our findings underscore the vulnerability of pipeline infrastructure to tropical cyclones (TCs) in general, and major hurricanes in particular. TCI intensity is a statistically significant predictor of both the likelihood and frequency of HMP failures during a storm, with failure frequency increasing exponentially for major hurricanes. The greatest increases in TC associated HMP failure are observed along the Texas and Mississippi coasts, where dense crude oil pipeline infrastructure intersects with exposure to intense TCs, including storm surges. The greatest overall likelihood of TC associated pipeline failure, invariant to TC intensity, is observed in the High Plains, perhaps due to tornado activity or the interaction between intense precipitation and soil expansion/contraction associated with shrink/swell clays present in the region. Lack of crude oil pipeline infrastructure equates to a significant reduction in overall HMP pipeline failure associated with extreme events on the Southeast coast, despite exposure to frequent, intense TCs. Historical data indicates that the annual maximum hurricane intersecting with hazardous material pipeline has increased from a Category 3 storm in 1970 to a Category 4 storm in 2010. Projecting this trend implies that a Category 5 hurricane can be expected to intersect with HMP infrastructure approximately annually by 2050, with strong implications for future HMP failure frequency across the eastern United States.

Though limited by lack of data, these findings strongly supports conclusions from previous research suggesting that TC-associated impacts to HMP infrastructure are under-reported in the literature, and stress the need for tailored risk assessments that incorporate complex contributions of natural hazards forcings, including TC forcings, to HMP failure occurrence in incident reports. If collected, such data could lend insight to improved preparedness measures and targeted mitigation strategies that are essential for safeguarding critical infrastructure against the increasing risks posed by expanding, aging pipeline networks intersecting with intensifying TCs under climate change.

Acknowledgments

Conflicts of Interest

The authors claim no conflicts of interest.

References

Abraham, J P et al. (2013). "A review of global ocean temperature observations: Implications for ocean heat content estimates and climate change: REVIEW OF OCEAN OBSERVATIONS". In: *Rev. Geophys.* 51.3, pp. 450–483. DOI: 10.1002/rog.20022.

Armstrong Jr, Martin F (1969). "The Natural Gas Pipeline Safety Act of 1968". In: *Nat. Resources Law.* 2, p. 142.

Awuku, Bright, Ying Huang, and Nita Yodo (2023). "Predicting natural gas pipeline failures caused by natural forces: An artificial intelligence classification approach". In: *Appl. Sci. (Basel)* 13.7, p. 4322. DOI: 10.3390/app13074322.

Belvederesi, Chiara, Megan S Thompson, and Petr E Komers (2018). "Statistical analysis of environmental consequences of hazardous liquid pipeline accidents". In: *Heliyon* 4.11, e00901. DOI: 10.1016/j.heliyon.2018.e00901.

Booth, James F et al. (2021). "Storm surge, blocking, and cyclones: A compound hazards analysis for the Northeast United States". In: *J. Appl. Meteorol. Climatol.* 60.11, pp. 1531–1544. DOI: 10.1175/jamc-d-21-0062.1.

Burow, Daniel, Kelsey Ellis, and Liem Tran (2021). "Simultaneous and collocated tornado and flash flood warnings associated with tropical cyclones in the contiguous United States". In: *Int. J. Climatol.* 41.8, pp. 4253–4264. DOI: 10.1002/joc.7071.

Carter, Elizabeth, Carolynne Hultquist, and Tao Wen (2023). "GRRIEn analysis: A data science cheat sheet for Earth scientists learning from global Earth observations". In: *Artificial Intelligence for the Earth Systems* 2.2, pp. 1–49. DOI: 10.1175/aies-d-22-0065.1.

Clayton, C R I et al. (2010). "Stresses in cast-iron pipes due to seasonal shrink-swell of clay soils". In: *Proceedings of the Institution of Civil Engineers - Water Management* 163.3, pp. 157–162. DOI: 10.1680/wama.2010.163.3.157.

Czajkowski, Jeffrey, Kevin Simmons, and Daniel Sutter (2011). "An analysis of coastal and inland fatalities in landfalling US hurricanes". In: *Nat. Hazards (Dordr.)* 59.3, pp. 1513–1531. DOI: 10.1007/s11069-011-9849-x.

Czajkowski, Jeffrey, Gabriele Villarini, et al. (2017). "Assessing current and future freshwater flood risk from north Atlantic tropical cyclones via insurance claims". In: *Sci. Rep.* 7, p. 41609. DOI: 10.1038/srep41609.

De Luca, Paolo et al. (2017). "Extreme multi-basin flooding linked with extratropical cyclones". In: *Environ. Res. Lett.* 12.11, p. 114009. DOI: 10.1088/1748-9326/aa868e.

Edwards, Roger (2021). "Tropical cyclone tornadoes: A review of knowledge in research and prediction". In: *Electron. J. Sev. Storms Meteorol.* 7.6, pp. 1–61. DOI: 10.55599/ejssm.v7i6.42.

Elsner, James B (2006). "Evidence in support of the climate change–Atlantic hurricane hypothesis". In: *Geophys. Res. Lett.* 33.16. DOI: 10.1029/2006GL026869.

— (2008). "Hurricanes and climate change". In: *Bull. Am. Meteorol. Soc.* 89.5, pp. 677–679.

F. Dormann, Carsten et al. (2007). "Methods to account for spatial autocorrelation in the analysis of species distributional data: a review". In: *Ecography (Cop.)* 30.5, pp. 609–628. DOI: 10.1111/j.2007.0906-7590.05171.x.

Gilford, Daniel M, Joseph Giguere, and Andrew J Pershing (2024). "Human-caused ocean warming has intensified recent hurricanes". In: *Environ. Res.: Climate* 3.4, p. 045019. DOI: 10.1088/2752-5295/ad8d02.

Girgin, S and E Krausmann (2016). "Historical analysis of U.S. onshore hazardous liquid pipeline accidents triggered by natural hazards". In: *J. Loss Prev. Process Ind.* 40, pp. 578–590. DOI: 10.1016/j.jlp.2016.02.008.

Girgin, Serkan and Elisabeth Krausmann (2014). "Analysis of pipeline accidents induced by natural hazards". In: *European Union: Brussels, Belgium.*

— (2015). "Lessons learned from oil pipeline natech accidents and recommendations for natech scenario development". In: *Institute for the Protection and Security of the Citizen. Elisabeth Krausmann, Address: Joint Research Centre, Via E. Fermi* 2749, p. 21027.

Guzman, Oscar and Haiyan Jiang (2021). "Global increase in tropical cyclone rain rate". In: *Nat. Commun.* 12.1, p. 5344. DOI: 10.1038/s41467-021-25685-2.

Holland, Greg and Cindy L Bruyère (2014). "Recent intense hurricane response to global climate change". In: *Clim. Dyn.* 42.3-4, pp. 617–627. DOI: 10.1007/s00382-013-1713-0.

International Energy Agency (2016). *Key world energy statistics 2016.* Key world energy statistics .. OECD. DOI: 10.1787/key_energ_stat-2016-en.

Knutson, Thomas et al. (2019a). "Tropical cyclones and climate change assessment: Part I: Detection and attribution". In: *Bull. Am. Meteorol. Soc.* 100.10, pp. 1987–2007. DOI: 10.1175/bams-d-18-0189.1.

— (2019b). "Tropical cyclones and climate change assessment: Part I: Detection and attribution". In: *Bull. Am. Meteorol. Soc.* 100.10, pp. 1987–2007. DOI: 10.1175/bams-d-18-0189.1.

Kossin, James P (2017). "Hurricane intensification along United States coast suppressed during active hurricane periods". In: *Nature* 541.7637, pp. 390–393. DOI: 10.1038/nature20783.

Kossin, James P et al. (2020). "Global increase in major tropical cyclone exceedance probability over the past four decades". In: *Proc. Natl. Acad. Sci. U. S. A.* 117.22, pp. 11975–11980. DOI: 10.1073/pnas.1920849117.

Lai, Yangchen et al. (2021). "Global compound floods from precipitation and storm surge: Hazards and the roles of cyclones". In: *J. Clim.* 34.20, pp. 1–55. DOI: 10.1175/jcli-d-21-0050.1.

Lam, Chio and Wenxing Zhou (2016). "Statistical analyses of incidents on onshore gas transmission pipelines based on PHMSA database". In: *Int. J. Pressure Vessels Piping* 145, pp. 29–40. DOI: 10.1016/j.ijpvp.2016.06.003.

Mallard, Megan S et al. (2013). "Atlantic hurricanes and Climate Change. Part I: Experimental design and isolation of thermodynamic effects". In: *J. Clim.* 26.13, pp. 4876–4893. DOI: 10.1175/jcli-d-12-00182.1.

Maxwell, Keely, Brittany Kiessling, and Jenifer Buckley (2018). "How clean is clean: a review of the social science of environmental cleanups". In: *Environ. Res. Lett.* 13.8, p. 083002. DOI: 10.1088/1748-9326/aad74b.

Michanowicz, Drew R et al. (2017). "A national assessment of underground natural gas storage: identifying wells with designs likely vulnerable to a single-point-of-failure". In: *Environ. Res. Lett.* 12.6, p. 064004. DOI: 10.1088/1748-9326/aa7030.

Murphy, John F and Jim Conner (2012). "Beware of the black swan: The limitations of risk analysis for predicting the extreme impact of rare process safety incidents". In: *Process Saf. Prog.* 31.4, pp. 330–333. DOI: 10.1002/prs.11524.

Nair, Gautam S, S Dash, and G Mondal (2018). "Review of Pipeline Performance during Earthquakes since 1906". In: *J. Perform. Constr. Facil.* 32.6, p. 04018083. DOI: 10.1061/(ASCE)CF.1943-5509.0001214.

NHC (2023). *Atlantic hurricane database (HURDAT2) 1851-2023.*

Olive, W W et al. (1989). *Swelling clays map of the conterminous United States.*

Parfomak, Paul W (2023). "DOT's federal pipeline safety program: Background and issues for congress". In: *Congressional Research Service.*

Pedregosa, Fabian et al. (2011). "Scikit-learn: Machine Learning in Python". In: *J. Mach. Learn. Res.* abs/1201.0490, pp. 2825–2830. DOI: 10.5555/1953048.2078195.

Pielke Jr, Roger A et al. (2005). "Normalized Hurricane Damage in the United States". In: *Nat. Hazards Rev.* DOI: 10.1061/(ASCE)1527-6988(2008)9:1(29).

Qin, Guojin et al. (2020). "Risk assessment for oil leakage under the common threat of multiple natural hazards". In: *Environ. Sci. Pollut. Res. Int.* 27.14, pp. 16507–16520. DOI: 10.1007/s11356-020-08184-7.

Qin, Rongshui, Nima Khakzad, and Jiping Zhu (2020). "An overview of the impact of Hurricane Harvey on chemical and process facilities in Texas". In: *Int. J. Disaster Risk Reduct.* 45.101453, p. 101453. DOI: 10.1016/j.ijdrr.2019.101453.

Reed, Kevin A, Michael F Wehner, and Colin M Zarzycki (2022). "Author Correction: Attribution of 2020 hurricane season extreme rainfall to human-induced climate change". In: *Nat. Commun.* 13.1, p. 2589. DOI: 10.1038/s41467-022-30242-6.

Restrepo, Carlos E, Jeffrey S Simonoff, and Rae Zimmerman (2009). "Causes, cost consequences, and risk implications of accidents in US hazardous liquid pipeline infrastructure". In: *Int. J. Crit. Infrastruct. Prot.* 2.1-2, pp. 38–50. DOI: 10.1016/j.ijcip.2008.09.001.

Ricci, Federica, Valeria Casson Moreno, and Valerio Cozzani (2021). "A comprehensive analysis of the occurrence of Natech events in the process industry". In: *Process Saf. Environ. Prot.* 147, pp. 703–713. DOI: 10.1016/j.psep.2020.12.031.

Sengul, Hatice et al. (2012). "Analysis of hazardous material releases due to natural hazards in the United States". In: *Disasters* 36.4, pp. 723–743. DOI: 10.1111/j.1467-7717.2012.01272.x.

U.S. Government Publishing Office. Title 49 - Transportation. Parts 191 - 195 (1970).

US Department of Transportation Pipeline and Hazardous Materials Safety Administration (2023). *Gas Distribution, Gas Gathering, Gas Transmission, Hazardous Liquids, Liquefied Natural Gas (LNG), and Underground Natural Gas Storage (UNGS) Annual Report Data.*

Vecchi, G et al. (2021). "Changes in Atlantic major hurricane frequency since the late-19th century". In: *Nat. Commun.* 12.1, p. 4054. DOI: 10.1038/s41467-021-24268-5.

Zakikhani, Kimiya, F Nasiri, and T Zayed (2020). "A review of failure prediction models for oil and gas pipelines". In: *Journal of Pipeline Systems Engineering and Practice* 11, p. 03119001. DOI: 10.1061/(asce)ps.1949-1204.0000407.

Intensifying tropical cyclones associated with more frequent hazardous material pipeline failures.

This version of the manuscript is a non-peer reviewed preprint that was submitted to EarthArXiv. Subsequent versions of this manuscript may have slightly different content.

M. Smith[1] and E. Carter[2]*

[1] Civil and Environmental Engineering, Cornell University, Ithaca, NY, USA
[2] Civil and Environmental Engineering, Syracuse University, Syracuse, NY, USA
*corresponding author
E-mail: ekcarter@syr.edu

Code and data:
Carter, E. & Smith, M. (2024). TC Pipelines, GitHub repository, https://github.com/LizCarter492/TCPipeline

Text S1: Data description

This analysis utilizes two data sets; the first being the PHMSA Distribution, Transmission & Gathering, LNG, and Liquid Accident and Incident Data for pipeline failures since 1970and the National Hurricane Center and Central Pacific Hurricane Center Best Track Data from the Atlantic Hurricane Database since 1851 (National Hurricane Center 2023).

The PHMSA Failure Dataset compiles all operator-generated incidence reports for gas distribution, gas transmission, and hazardous liquid pipelines starting in 1970 (gas distribution, gas transmission). The PHMSA pipeline failure reporting consists of four different reports for each pipeline transmission type reflective of the evolving reporting criteria since the implementation of the reporting regulation. The original regulation (PHMSA 2014) for incident report criteria in 1970 outlined the criteria for an "incident" as: 1) any leak that caused death or personal injury, 2) a leak from a pipeline that required the segment to be taken out of service, 3) a gas ignition incident, 4) an incident that caused damage of $50,000 or more, or 5) an incident that was a significant occurrence through the judgment of the operator. Since the original regulation criteria were set 50 years ago, there have been 7 amendments to these criteria. Each change was made to more clearly outline what is considered a reportable incident. The current definition of an incident is 1) a reportable event that leads to death or personal injury, 2) an event that causes property damage of $122,000 or more, 3) an unintentional loss of 3 million cubic feet or more of gas, 4) an event that results in an emergency shutdown on a Liquified Natural Gas facility, or 5) an event that is significant in the judgment of the operator. The evolving nature of the definition of an event underscores the complexity of working with PHMSA data in quantifying temporal trends in pipeline failures.

The NOAA HURDAT2 Dataset, compiled by the National Hurricane Center (NHC), evaluates all available observations (real time and post-hoc) to generate an official assessment of the history of all tropical cyclones originating in the Atlantic Ocean following recommendations of the Best Track Change Committee (National Hurricane Center 2023). For each unique tropical and subtropical cyclone recorded since 1949, the NOAA HURDAT2 dataset details six hourly increments, latitude, longitude, category, maximum wind, and central pressure. From 2004 to present, the NOAA HURDAT2 additionally details the TC force diameter (National Hurricane Center 2023) for each storm.

Due to changing reporting criteria in the PHMSA dataset, there are inconsistencies of and within the variables reported. Only pipeline characteristics that remain consistent

Supplementary Information

over the 50 years of the PHMSA failure reports are considered for this analysis. These include the failure date, location, and cause of failure. All PHMSA records include county and state of incident, most provide the municipality, and many include a precise longitude and latitude of failure point. For records without a latitude and longitude of failure point, the provided address was used to geolocate the associated latitude and longitude coordinates using a google maps key (Google 2023).

Operators filing PHMSA incident reports are instructed to select one cause from a number of pre-prescribed causes of failure. As cause of failure categories on incident reports have changed over time, and as many pipeline failures may have one or more overlapping causes (i.e. corrosion and natural force damage), PHMSA failure cause categories are aggregated into three types that are of interest to this analysis. The first category is meant to capture failures associated with *human error*, including construction/operator errors, excavation damage, and other operator errors. Human errors are expected to occur independently of TC forcings. The second category captures a wide array of *mechanical failures* associated with some outside forcing, including malfunction of equipment, material/weld failures, and outside force damage. Mechanical failures may or may not be associated with TC forcings. The third category is *natural force damages*, a category that is adopted in the PHMSA Failure Dataset starting in 2002. In theory, natural force damages ostensibly includes damages directly associated with TCs after 2002. Trends in the frequency of human errors, mechanical failures, and natural forcing failure frequencies over time are evaluated using simple linear regression. The data obtained from the NOAA HURDAT2 Dataset is originally formatted in a comma-delimited text format and was processed into an effective format using the Best Track Data code through GitHub from Metemaad (Etemad 2024).

Data Preparation Details

The data preparation process involved several critical steps to ensure accurate analysis of pipeline failure causes and locations. Here, we describe the methods used for attributing causes to failure categories, applying k-means clustering, and classifying spatial data.

Attributing Failure Causes

Initially, we categorized pipeline failures into specific groups based on their causes. This categorization helps in understanding the predominant factors leading to failures. We used predefined criteria to map various causes into three broad categories: 'outside', 'human', and 'natural'. For instance, causes such as "DAMAGE BY OUTSIDE FORCES," "CONSTRUCTION DEFECT/MATERIAL FAILURE," and "CORROSION" were grouped under 'outside'. Causes attributed to operator errors or mishandling, like "CONSTRUCTION/OPERATING ERROR" and "INCORRECT OPERATION," were classified as 'human'. Natural phenomena, such as "NATURAL FORCES," were placed in the 'natural'

Supplementary Information

category. This systematic categorization streamlined the analysis and interpretation of the data.

Spatial Data Preparation and Clipping

To analyze the geographical distribution of pipeline failures, we began by loading a geospatial dataset representing countries and continents. We specifically focused on the United States and North America for detailed analysis. Using GeoPandas, we converted our dataset into a GeoDataFrame, specifying the coordinates for each pipeline failure event. The coordinate system used was EPSG:4326, a common standard for geospatial data.

We then performed a spatial clipping operation to isolate pipeline failures within a buffer zone around the United States. This buffer zone was chosen to include areas slightly beyond the country's borders to capture any relevant incidents. By clipping the data, we ensured that only the failures within this region were included in subsequent analyses. This step was essential to maintain focus on the geographic area of interest and eliminate irrelevant data points.

K-Means Clustering for Spatial Classification

To identify patterns and clusters in the geographic distribution of pipeline failures, we applied the k-means clustering algorithm. This method grouped the failure incidents into six clusters based on their latitude and longitude. We used a random state for reproducibility and ensured the clustering process was stable and consistent by setting the number of initializations appropriately.

Once the clustering was completed, each pipeline failure incident was assigned to a specific location group. This categorization allowed us to visualize and analyze the spatial distribution of failures more effectively. The clusters provided insights into potential hotspots and regional variations in pipeline failure occurrences.

Visualization of Results

The results of our spatial and clustering analyses were visualized using maps. For the initial spatial distribution, we plotted the pipeline failures on a map of North America, highlighting the regions with incidents. Different colors represented the presence or absence of failures.

For the clustering results, we created another map showing the geographic clusters of pipeline failures. Each cluster was depicted in a distinct color, allowing us to identify and examine spatial patterns. These visualizations were crucial in conveying the analysis outcomes and facilitating a deeper understanding of the spatial dynamics of pipeline failures.

Supplementary Information

By following these detailed data preparation steps, we ensured a robust foundation for analyzing pipeline failures and deriving meaningful insights.

Text S2: Binomial Mixed-Effects Model

For the binomial mixed-effects model, the response variable was binary, indicating whether there was at least one pipeline failure or none. The dataset was adjusted so that any occurrence of one or more failures was coded as 1, while no failures were coded as 0.

We trained two binomial models:

1. A null model (mb1) with only random intercepts for location (locGrp) and year (yr).
2. A trained model (mb2) including the first principal component of hurricane characteristics (TCI) as a fixed effect along with random intercepts for location and year.

The binomial model fitting used the logit link function to estimate the probability of at least one failure. The inclusion of TCI in the model allowed us to assess the influence of hurricane characteristics on the likelihood of pipeline failures.

Text S3: Poisson Mixed-Effects Model

For the Poisson mixed-effects model, the response variable was the count of pipeline failures. The Poisson distribution is appropriate for count data, especially when the data includes many zeroes, as in our case.

We trained two Poisson models:

3. A null model (m1) with only random intercepts for location and year.
4. A trained model (m2) including TCI as a fixed effect along with random intercepts for location and year, and a random intercept for TCI on location.

The Poisson model fitting used the log link function to predict the expected number of failures. This model allowed us to quantify the relationship between hurricane characteristics and the frequency of pipeline failures.

Text S4: Principal Component Analysis (PCA)

Tropical cyclone characteristics are highly collinear (Figure S3), which could contribute to model instability and biased estimates. In order to define a single index of tropical cyclone intensity that captured the majority of the information content of different meteorological descriptors of hurricane strength, we performed a Principal Component Analysis (PCA) on

Supplementary Information

three key variables: maximum windspeed, minimum pressure, and minimum latitude. The hurricane data was normalized before applying PCA to ensure all variables were on a comparable scale. The first principal component (PC1), capturing nearly 70% of the variance in these three characteristics (Figure S4), was extracted and added to the dataset as the variable TCI to be used as the predictor variable.

Text S5: Variance Component Partitioning

Parameter estimates for both binomial and Poisson models were obtained using the glmer function from the lme4 package, which fits generalized linear mixed-effects models. By comparing the null models to the trained models, we could partition the variance and determine how much of the temporal and spatial variance in pipeline failures was explained by hurricane characteristics.

Variance partitioning involved calculating the reduction in variance for the random effects (location and year) when fixed effects (hurricane characteristics) were included in the model. This comparison provided insights into the extent to which hurricane characteristics influenced pipeline failures.

We evaluated the statistical significance of the fixed effects (TCI) in both the binomial and Poisson models by examining the p-values and confidence intervals of the parameter estimates. Additionally, model validation involved assessing the goodness-of-fit and examining residuals to ensure no major deviations from model assumptions.

For the binomial model, the log odds ratio of the fixed effect was converted to an odds ratio to interpret the increase in likelihood of at least one failure per standard deviation increase in TCI. For the Poisson model, the predicted counts were compared to observed counts, and residual plots were examined to validate model fit.

Text S6: Justification for Model Choices

The choice of mixed-effects models was driven by the hierarchical structure of the data, with multiple failure records nested within locations and years. This structure warranted the use of random intercepts to account for the non-independence of records. The use of binomial and Poisson distributions addressed the nature of the response variables: binary for occurrence and count for frequency of failures, respectively. The inclusion of principal components as fixed effects allowed us to succinctly incorporate multiple correlated hurricane characteristics into the models.

By training and comparing these models, we aimed to quantify the impact of hurricane characteristics on pipeline failures while accounting for spatial and temporal dependencies in the data.

Supplementary Information

Text S7: Justification for statistical hurricane strength predictions

Global climate models show substantial negative bias in the prediction of historic hurricane intensity and frequency, due in part to theoretical weaknesses in deterministic characterizations of hurricane-forming processes, and in part to the fact that hurricane-forming processes, and associated phenomena such as TC-associated hurricanes and convective storms, occur below the spatial resolution of many numerical climate models (Zhang et al. 2011). Historical negative bias in extreme TC prediction translates to high uncertainty in future numerical predictions of hurricane dynamics associated with global warming (Knutson et al. 2020). Alternatively, numerous empirical studies have documented strong trends in historical hurricane data parameters that are consistent with expectations for observed global warming in the late 20th and early 21st centuries (Knutson et al. 2019; Vecchi et al. 2021). As a result, we infer global-warming associated trends directly from NOAA HURDAT2 Dataset.

Historical Trends and Predictions

The linear regression analysis revealed significant trends in TC characteristics over the historical period. The slope and intercept of the regression lines were used to predict TC characteristics for the year 2050, assuming the trends observed from 1970 to 2022 continue.

For each characteristic, the regression model yielded a slope (rate of change per year) and an intercept (value at the start of the period). These values were used to project future TC characteristics:

- **Windspeed**: The slope and intercept from the regression model were used to predict the maximum windspeed in 2050.
- **Pressure**: Similarly, the slope and intercept predicted the minimum pressure in 2050.
- **Latitude**: The slope and intercept provided predictions for the minimum latitude in 2050.

Assumptions for Future Predictions

The future predictions assume that the coefficients from the historical regression models will remain constant until 2050. This assumption simplifies the projection by suggesting that the factors driving historical trends will continue to influence TC characteristics in the same manner. The significant linear trends observed from 1970 to 2022 are primarily attributed to global warming, implying that TC intensification trends due to global warming will persist.

Impact of Climate Change on TC Intensification

Climate change is expected to intensify TCs, resulting in higher maximum wind speeds and lower minimum pressures. These changes have direct implications for pipeline failure rates, as more intense TCs are likely to increase the frequency and severity of failures. The linear trends observed in the historical data suggest that if global warming continues at its current rate, TCs will become progressively more intense, thereby posing a greater risk to pipeline infrastructure.

Predicting Future Pipeline Failures

Using the historical trends, the predicted TC characteristics for 2050 were transformed into a combined hurricane component (TCI) representing the overall intensity of future TCs. This value was then used to make predictions with the trained failure models.

5. **Transformation into PC Space**: The predicted values for windspeed, pressure, and latitude in 2050 were standardized using the historical mean and standard deviation of each characteristic. These standardized values were combined to compute the TCI value for 2050.
6. **Prediction with Failure Models**: The TCI value for 2050 was used as an input to the binomial and Poisson mixed-effects models to predict future pipeline failures. The models incorporated the random effects of location and year to provide nuanced predictions.
7. **Binomial Model Predictions**: The binomial model predicted the probability of at least one pipeline failure for different location groups in 2050. This provided insights into the likelihood of pipeline failures under intensified TC conditions.
8. **Poisson Model Predictions**: The Poisson model predicted the expected number of pipeline failures for different location groups in 2050. This helped estimate the frequency of failures based on future TC intensification.

Justification for Using Historical Trends

The use of historical trends to project future TC characteristics is justified by the strong linear relationships observed in the data, and for lack of a robust alternative (e.g. numerical) modelling framework capable of capturing the impact of thermodynamic and dynamic intensification on TC propagation. These relationships indicate a consistent pattern of TC intensification over the past decades, likely driven by global warming. By assuming that these trends will continue, we can make naïve but useful predictions about future pipeline failure rates and plan accordingly to mitigate risks.

In conclusion, the OLS regression methods provided a reasonable framework for analyzing historical trends in TC characteristics and projecting future changes. The predictions,

Supplementary Information

based on the assumption of continued linear trends, highlight the potential impact of climate change on TC intensity and pipeline failure rates. These insights are critical for developing strategies to enhance the resilience of pipeline infrastructure in the face of evolving climatic conditions.

Text S7: Binomial Mixed-Effects Model

To compare the null model (mb1) with the full model (mb2) and interpret the key aspects, several outputs must be considered: the Akaike Information Criterion (AIC), the variance components, and the fixed effects.

The AIC is a measure of the relative quality of a statistical model for a given dataset, providing a means for model selection. In the null model (mb1), the AIC is 351.2 with a log-likelihood (logLik) of -172.6, while in the full model (mb2), the AIC is 337.9 with a log-likelihood of -165.0. The difference in AIC (ΔAIC) is calculated as 351.2 - 337.9 = 13.3. A lower AIC in the full model indicates a better fit to the data compared to the null model. Typically, a ΔAIC greater than 10 suggests strong evidence in favor of the model with the lower AIC, supporting the superiority of the full model in this case.

The variance components reveal how much of the variance in the data is explained by the inclusion of TCI. In the null model, the year variance is 0.19680 and the location group variance is 0.08209. In the full model, the year variance is slightly reduced to 0.1964, and the location group variance decreases to 0.0642. The reduction in location group variance is calculated as (0.08209 - 0.0642) / 0.08209 = 0.217 or 21.7%, indicating that TCI accounts for a significant portion of the variability in pipeline failures across different locations.

Examining the fixed effects in the full model, the intercept is -1.51715, which is significant with $p<0.001$, and the coefficient for TCI is 0.35611, also significant with $p<0.001$. The intercept represents the log-odds of pipeline failure when TCI is zero. The positive coefficient for TCI suggests that for each unit increase in TCI, the log-odds of pipeline failure increase by 0.35611. Converting the log-odds to an odds ratio, $\exp^{(0.35611)} \approx 1.428$, implies that a one-unit increase in TCI is associated with a 42.8% increase in the odds of pipeline failure.

The range of scaled residuals provides insights into the model fit. In the null model, the scaled residuals range from -0.7287 to 2.4722, while in the full model, they range from -1.1591 to 3.2242. Although the full model still exhibits some large residuals, suggesting that other factors not included in the model may affect pipeline failures, the overall fit is improved (Figure S9).

Supplementary Information

In summary, the full model (mb2) with an AIC of 337.9 fits the data significantly better than the null model (mb1) with an AIC of 351.2. The inclusion of TCI reduces the location group variance by 21.7%, highlighting its substantial role in explaining pipeline failures. The coefficient for TCI in the full model indicates that an increase in hurricane intensity is significantly associated with a 42.8% increase in the odds of pipeline failure. Despite some large residuals, the fixed effects and random effects in the full model underscore the importance of TCI in understanding pipeline failures.

Text S8: Poisson Mixed-Effect Model

To compare the null model (m1) with the full model (m2) and interpret the key aspects, several outputs must be considered: the Akaike Information Criterion (AIC), the variance components of the random effects, and the fixed effects.

The AIC is a measure used to compare models, with a lower AIC indicating a better fit. In the null model (m1), the AIC is 1042.3 with a log-likelihood (logLik) of -518.1, while in the full model (m2), the AIC is 917.1 with a log-likelihood of -454.5. The difference in AIC (ΔAIC) is calculated as 1042.3 - 917.1 = 125.2. This substantial reduction in AIC strongly indicates that the full model (m2) with the TCI variable fits the data much better than the null model (m1).

The variance components reveal how much of the variance in the data is explained by the inclusion of TCI. In the null model, the year variance is 1.5176 and the location group variance is 0.6266. In the full model, the year variance is reduced to 1.002, and the location group variance decreases to 0.475. The reduction in location group variance is calculated as (0.6266 - 0.475) / 0.6266 = 0.242 or 24.2%, indicating that TCI accounts for a significant portion of the variability in pipeline failures across different locations.

Examining the random effects further, the inclusion of TCI also reduces the year variance by 34%. This is calculated as (1.5176 - 1.002) / 1.5176 = 0.34, showing that TCI explains a substantial portion of the variability in pipeline failures over time.

The fixed effects in the full model show that the intercept is -1.13571, which is significant with p=0.00115, and the coefficient for TCI is 0.46386, significant with p value. The intercept represents the log count of pipeline failures when TCI is zero. The positive coefficient for TCI suggests that for each unit increase in TCI, the log count of pipeline failures increases by 0.46386. Converting the log count to a multiplicative effect, $\exp^{(0.46386)} \approx 1.59$, means that a one-unit increase in TCI is associated with a 59% increase in the expected count of pipeline failures.

The range of scaled residuals provides insights into the model fit. In the null model, the scaled residuals range from -2.5195 to 9.7870, while in the full model, they range from -

Supplementary Information

2.3313 to 7.9828. Although the full model still exhibits some large residuals, suggesting potential outliers or other factors not accounted for in the model, the overall fit is improved (Figure S9).

In summary, the full model (m2) with an AIC of 917.1 fits the data significantly better than the null model (m1) with an AIC of 1042.3. The inclusion of TCI reduces the location group variance by 24.2% and the year variance by 34%, highlighting its substantial role in explaining pipeline failures. The coefficient for TCI in the full model indicates that an increase in hurricane intensity is significantly associated with a 59% increase in the expected count of pipeline failures. Despite some large residuals, the fixed effects and random effects in the full model underscore the importance of TCI in understanding pipeline failures.

Text S9: Detailed explanation of v_k anomalies in Poisson regression

The years of 2014, 2005, 2017, 1992, and 2012 all demonstrated high TC associated failure frequencies by way of null intercept, and indicate that TC intensity was highly important in predicting these anomalies (Figure 3). In 2014, Hurricane Arthur intersected with 5 anomalous failures in the Northeast; more than might be expected in the region for a peak Category 2 storm. In 2005 Hurricane Katrina intersected with 30 failures (26 in the MI Delta) and Hurricane Rita intersected with 44 failures (18 in the Texas Coast, 11 in the MI Delta, and 10 in the High Plains). In 2017, 54 failures intersected with Hurricane Harvey (42 in the Texas Coast), and 13 intersected with Hurricane Nate (6 in the MI Delta); in 1992 14 failures intersected with Hurricane Andrew (6 in the MI Delta). Apparent trends in random intercepts on year indicate that HMP sensitivity to TCI is increasing over time, invariant of other drivers of increased HMP , such as age of pipes.
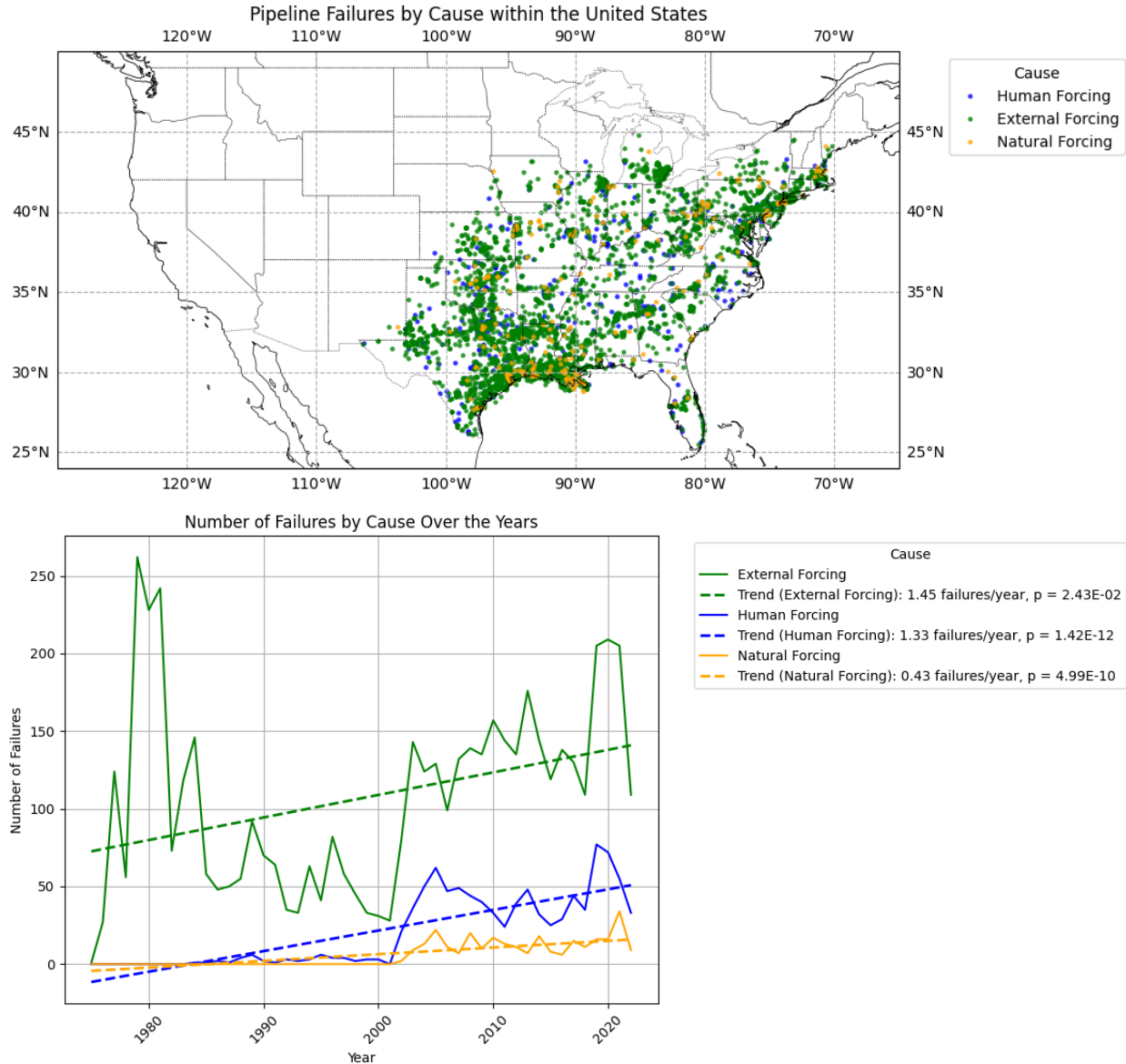
Supplementary Information

Figure S1: PHMSA failure cause categories are aggregated into three types that are of interest to this analysis. The first category is meant to capture failures associated with *human error*, including construction/operator errors, excavation damage, and other operator errors. Human errors are expected to occur independently of TC forcings. The second category captures a wide array of *mechanical failures* associated with some outside forcing, including malfunction of equipment, material/weld failures, and outside force damage. Mechanical failures may or may not be associated with TC forcings. The third category is *natural force damages*, a category that is adopted in the PHMSA Failure Dataset starting in 2002. In theory, natural force damages ostensibly includes damages directly associated with TCs after 2002. (Top) Pipeline failures since 1985 within 300 miles of a TC track, categorized by cause of failure as attributed on PHMSA database. (Bottom) Frequency of pipeline failures since 1985 categorized by cause of failure.

Supplementary Information
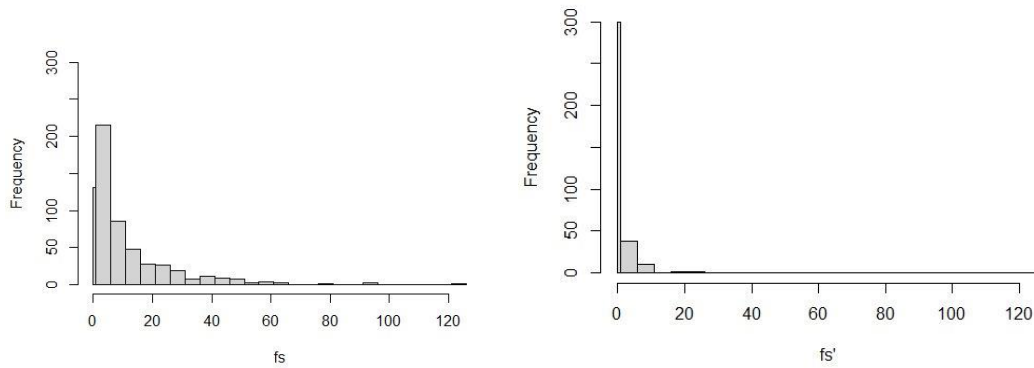
Figure S2: Histogram of storm associated failure frequency (fs) and storm-related failure frequency (fs')
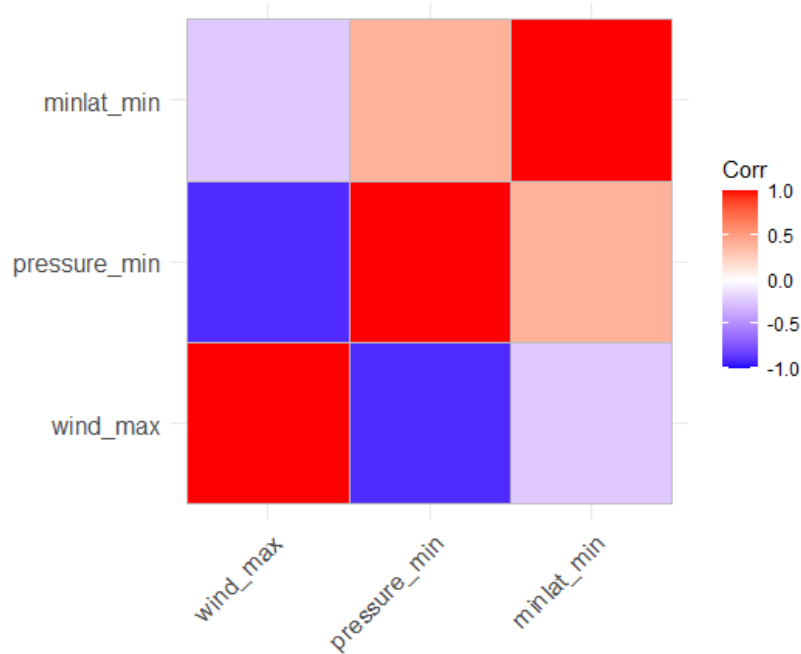

Figure S3: Correlogram of HMP region maximum tropical cyclone pressure (pressure_min), HMP minimum tropical cyclone windspeed (wind_max), and overall storm minimum latitude.
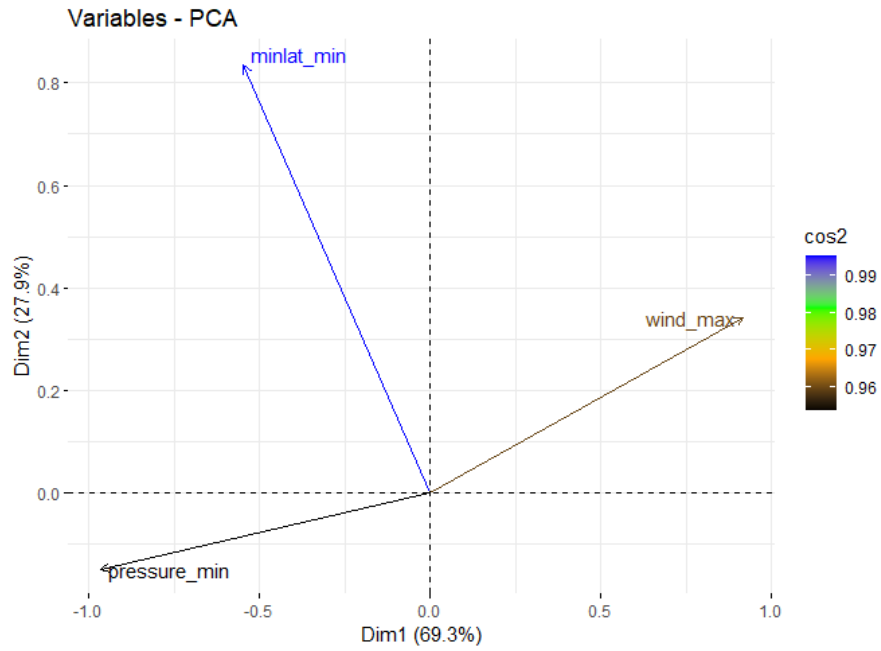
Supplementary Information

Figure S4: Principal Component Analysis bi-plot of tropical cyclone maximum windspeed per HMP region (wind_max), minimum pressure per HMP region (pressure_min) and minimum latitude per storm (minlat_min). Dim 1 corresponds to tropical cyclone intensity (TCI).

Supplementary Information
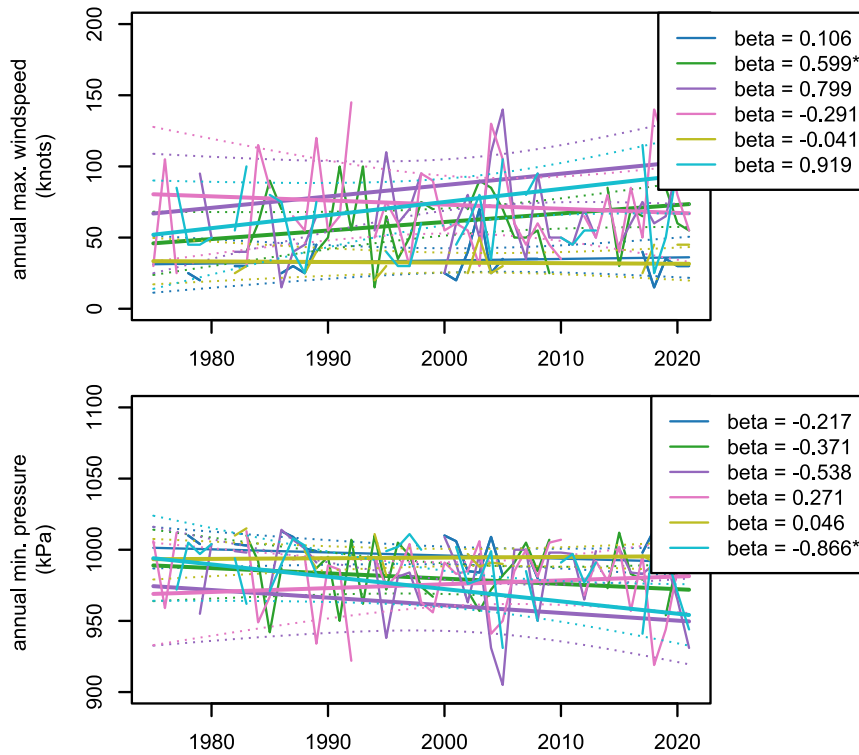
Figure S5: Time series of HMP regional annual maximum TC windspeed (top), minimum pressure (middle), and minimum storm latitude (bottom), with linear trendlines and 95% confidence interval overlaid; linear coefficients shown in legend. Color scale indicates HMP region, consistent with colors used on figures in main text.
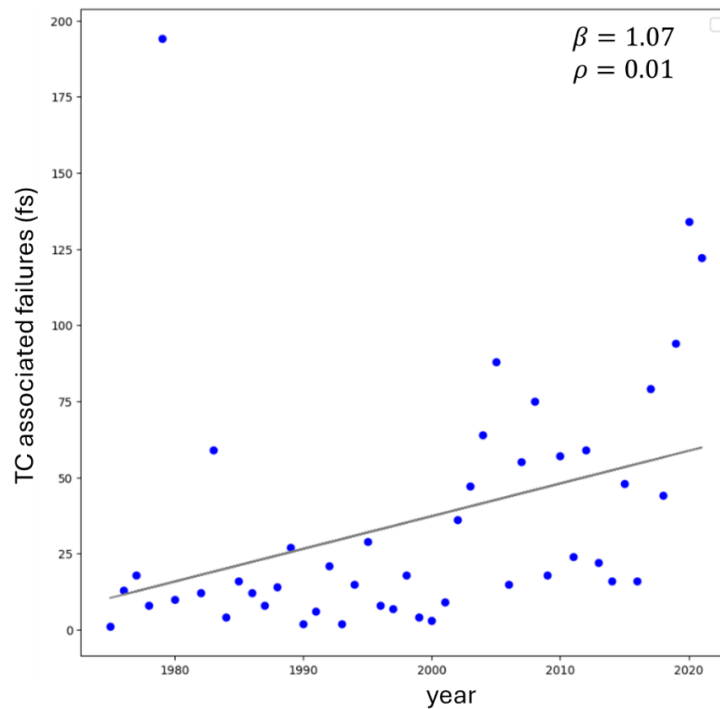
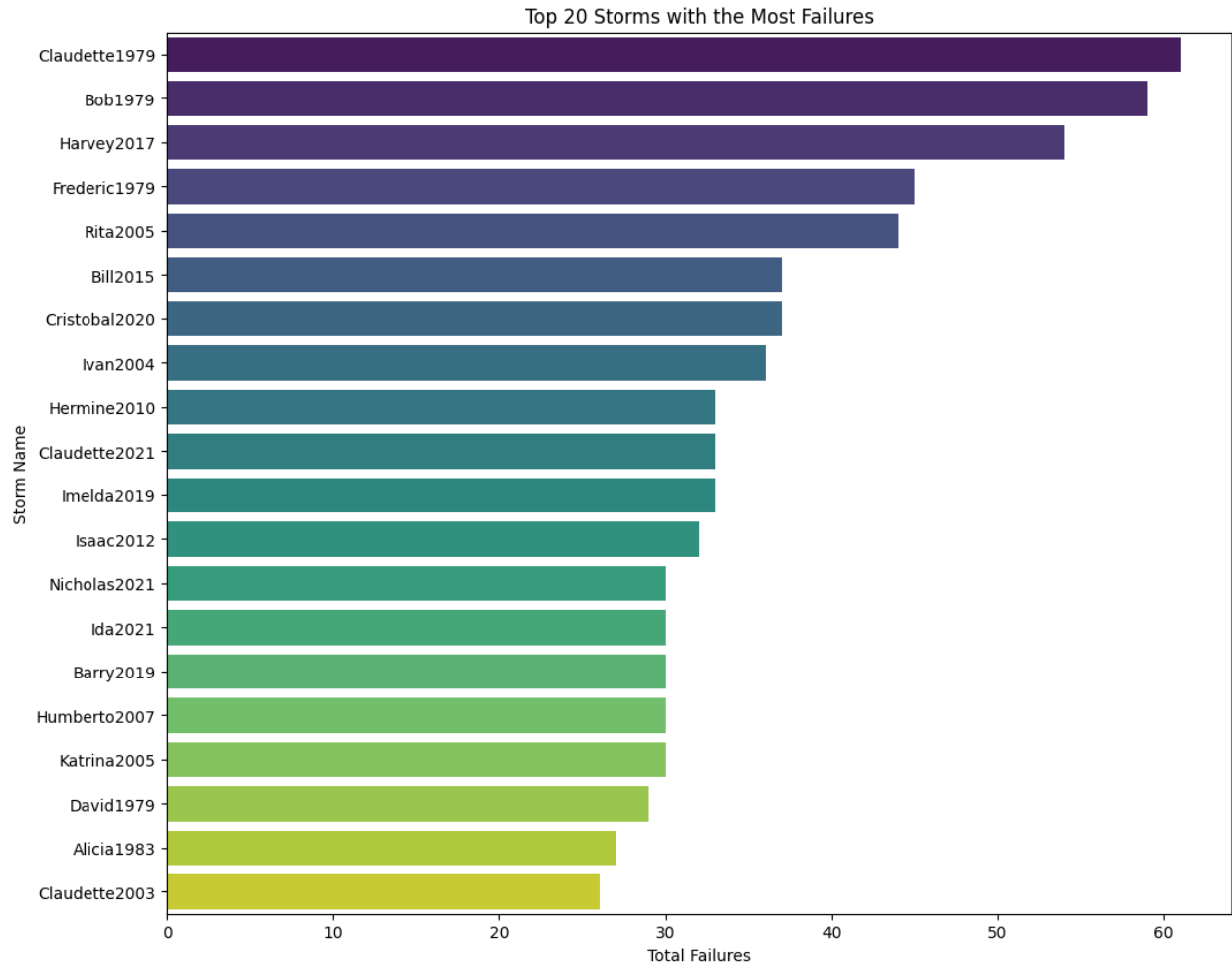
Figure S6: Trend in annual cumulative fs over time.

Supplementary Information

Figure S7: Twenty storms associated with the most HMP failures.
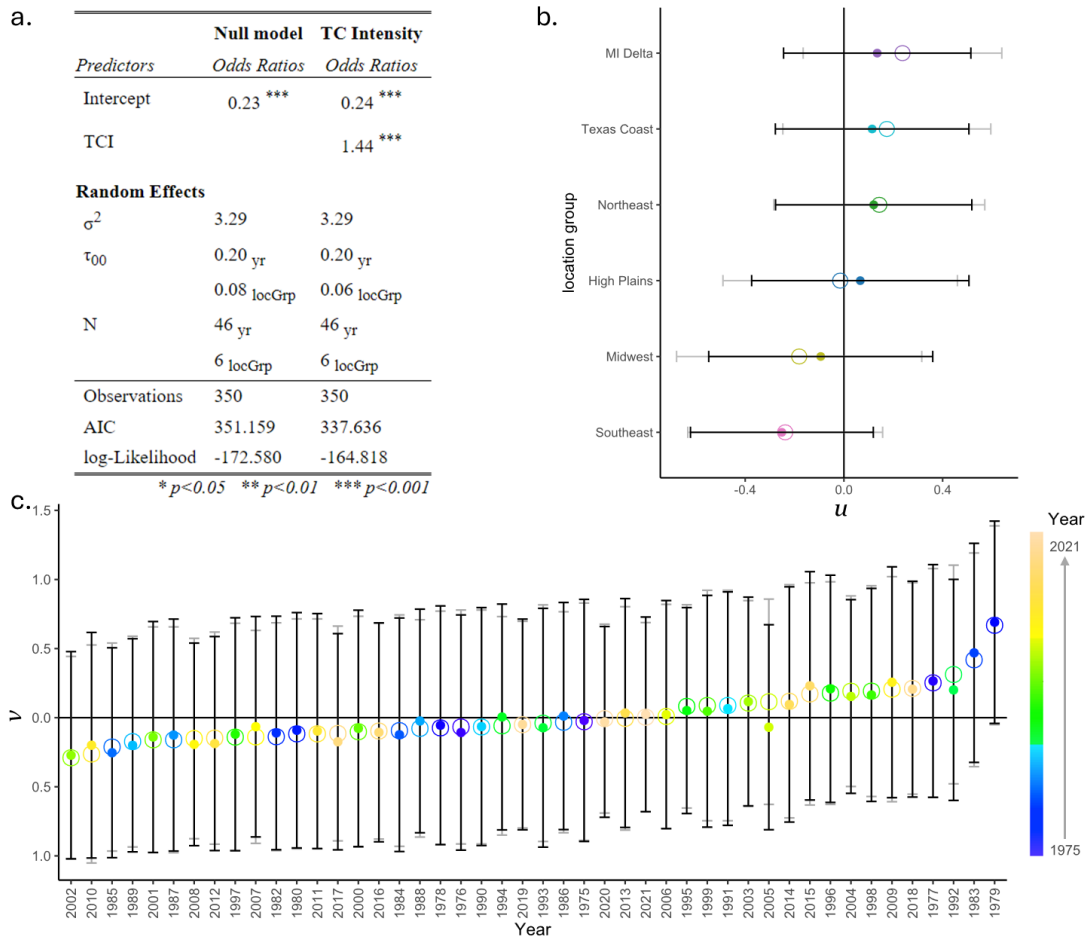
Supplementary Information

Figure S8: a) Mixed-effects binomial model parameters and statistics for null (no fixed effects) and full (TCI as a fixed effect) models, b) caterpillar plot of random intercept (points) on location for null (open circles) and full (closed circles) models, with error bar representing 95% confidence interval; color scale indicating location group c) as in b but for random intercept on year, with color scale indicating advancing year.
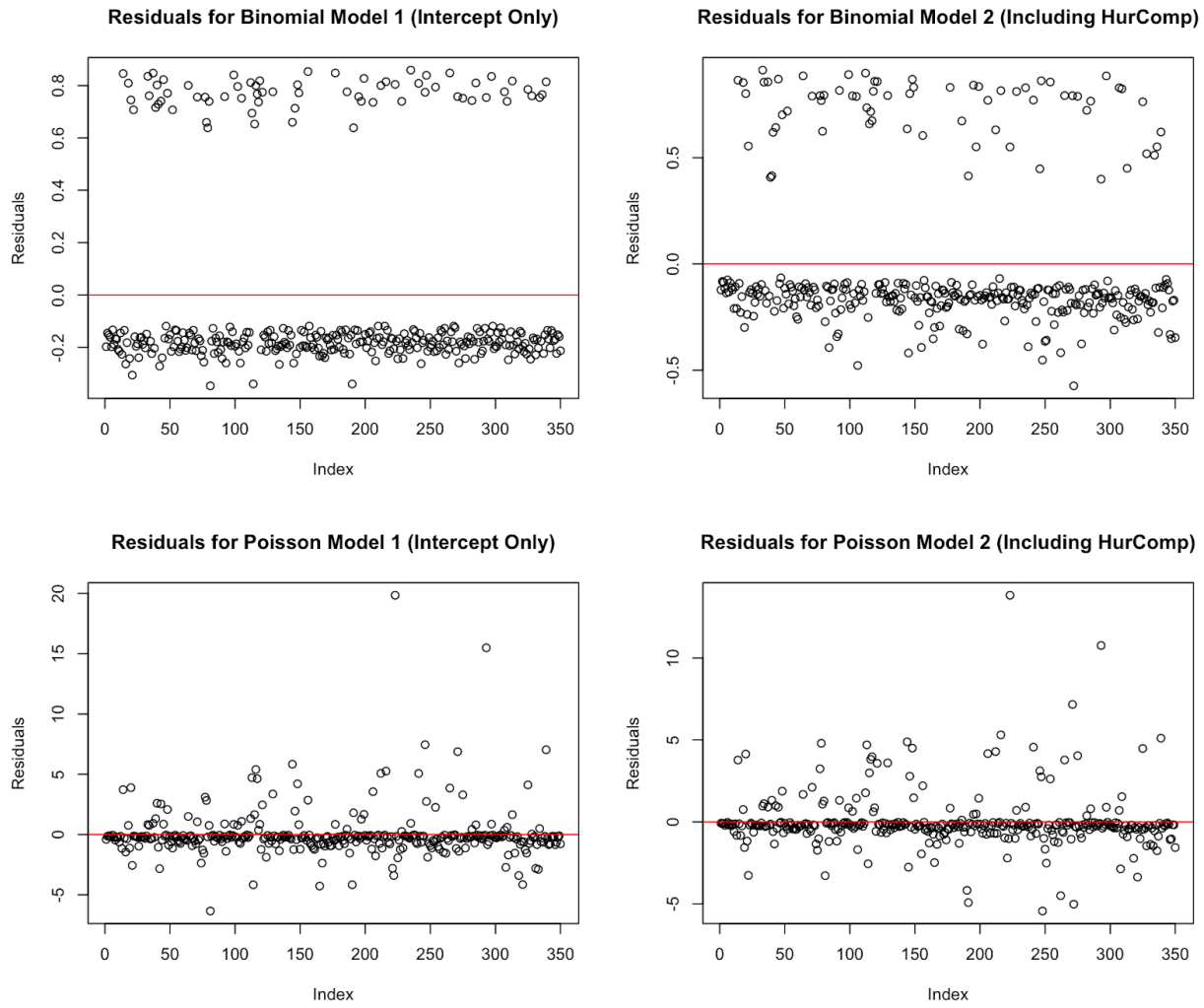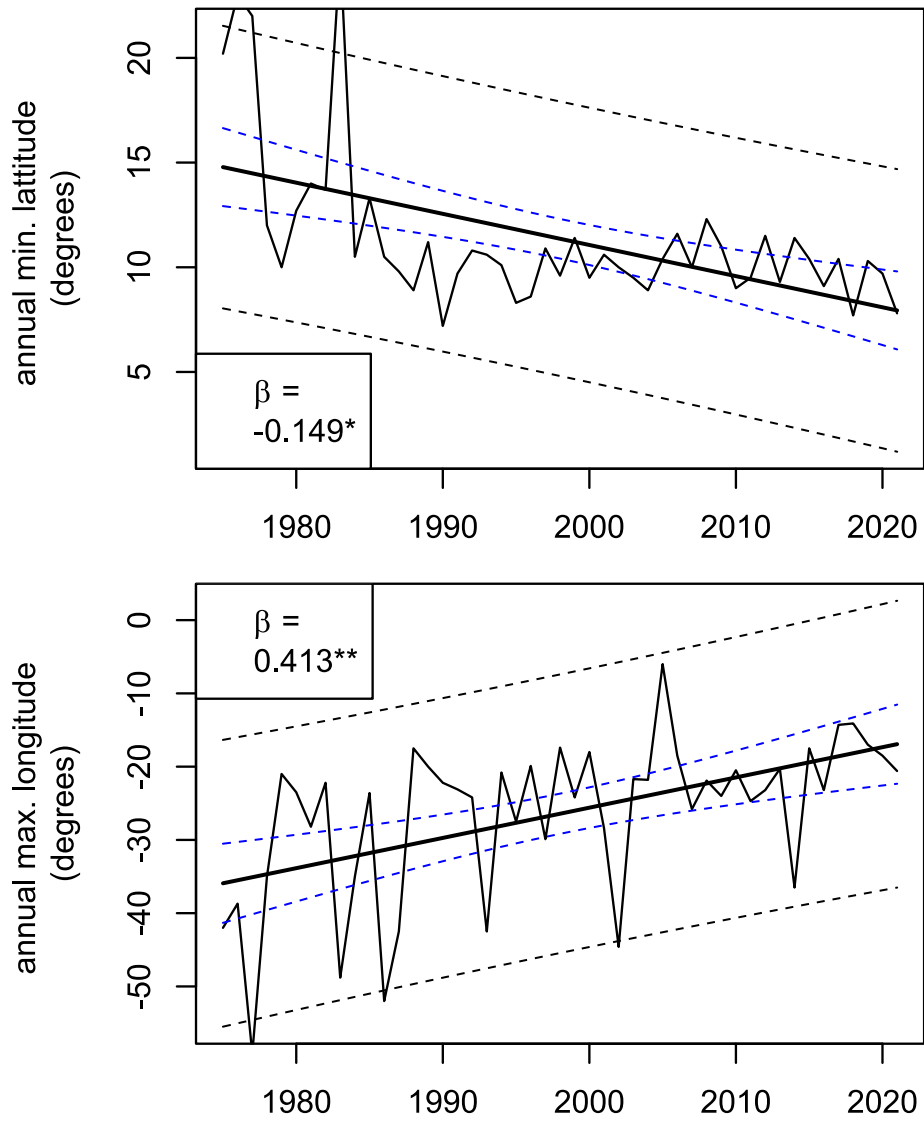
Figure S9: Binomial and Poisson Model residuals.

Supplementary Information

Figure S10: Trends in southeastern most originating TC from 1975-2022